Sensitivity of simulated storm life span to ventilation parameterization in a cloud resolving model

Yen-Liang Chou[1], Pao K. Wang[1,2,3,4,*], and Kai-Yuan Cheng[5]

[1] Research Center for Environmental Changes, Academia Sinica, Taipei City, Taiwan
[2] Department of Aeronautics and Astronautics, National Cheng Kung University, Tainan City, Taiwan
[3] Department of Atmospheric Science, National Taiwan University, Taipei City, Taiwan
[4] Department of Atmospheric and Oceanic Sciences, University of Wisconsin-Madison, Madison, Wisconsin, USA
[5] Program in Atmospheric and Oceanic Sciences, Princeton University, and NOAA/Geophysical Fluid Dynamics Laboratory, Princeton, New Jersey, USA

ABSTRACT

We perform a sensitivity study on the ventilation effect of large hydrometeors, namely, raindrops, snow aggregates, and hail in a cloud-resolving model. The ventilation effect could accelerate the heat and mass transfer rates between vapor and falling hydrometeors. It causes the falling hydrometeors to grow (in a supersaturated environment) and dissipate (in a subsaturated environment) faster than the stationary ones. The parameterizations of the ventilation effect on hydrometeors in a cloud model is critical as it could dramatically alter the structure and the lifespan of the simulated storm. Enhancing the ventilation coefficients of falling hydrometeors leads to a longer-lived storm featured by apparent storm splitting. The temporal evolution of hail density fluctuates greater than the default case (the control case) indicating both stronger deposition and sublimation in hail microphysical processes. However, both rainfall and hailfall become less intense than the control run. In contrast, reducing the ventilation effect causes moderate evaporation of raindrops as they fall through subsaturated air. Consequently, the concentration and precipitation rate of raindrops increase near the surface. Strong downdraft accompanying the heavy rainfall cuts off the low-level inflow of unstable moist air into the storm and results in early dissipation of the storm.

1. INTRODUCTION

During the development of a cloud, its constituent hydrometeors, either water drops or ice particles or both, are constantly moving relative to the environmental air. This relative motion causes a special effect, called the ventilation effect, in heat and mass transfer between the hydrometeors and air. When a hydrometeor is growing by addition of water vapor in a supersaturated environment (the diffusion growth mode), the mass transfer rate of vapor towards the hydrometeor will be enhanced by a factor as compared to the situation when there is no relative motion between the hydrometeors and air. This enhancement factor is called the ventilation coefficient. In addition, latent heat will be released to the environmental air during this growth process

as there is a phase change of water substance (net change of vapor into liquid phase). The heat transfer rate will be enhanced by a ventilation coefficient as well because the hydrometeor is moving. When this same hydrometeor is evaporating, its evaporation rate and the environmental cooling rate (due to the consumption of latent heat by phase change) will also be enhanced by the same coefficient as long as it moves at the same velocity (Pruppacher and Klett 1997; Wang 2013).

The enhanced heat and mass transfer rates obviously will have significant impact on the cloud development process. If we assume the hydrometeors are stationary, the amount of latent heat release during the rapid growth phase of moving hydrometeors would be severely underestimated whereas in reality the latent heat release should be much larger and hence the cloud growth would be much

---

* Corresponding author
  E-mail: pkwang@gate.sinica.edu.tw

more vigorous. Similarly, the cooling effect due to the large falling hydrometeors (large raindrops, hailstones) can be very large (Wang 2013; Cheng et al. 2014) and the cold air produced in such a rapid cooling environment potentially can induce dangerous microburst that causes the crash of aircraft trapped in it (Fujita 1978), and this strong cooling wouldn't be able to be predicted correctly if we do not include accurate ventilation effect in the estimate.

Due to the difficulties and danger involved in direct in-situ observations of severe storms, currently one of the most viable ways of understanding the development of thunderstorms is using a physics-based cloud model with adequate built-in cloud microphysical processes to simulate real cases of thunderstorms and, if the simulation results look reasonable, perform analysis on the results to study the storm physics. This avoids the difficulties and danger of direct in-situ observation; however, the model physics must be carefully examined to make sure that they are reasonable enough. At the current stage, it is impractical to include the precise cloud microphysical processes which are mostly represented by time-dependent partial differential equations (Pruppacher and Klett 1997; Wang 2013) that require enormous computing resource to solve numerically. Instead the usual practice is to use parameterizations - representing microphysical processes by simple algebraic equations – to reduce the need of excessive computing resource.

There are many ways of doing cloud microphysical parameterizations and many papers are devoted to this subject and many are summarized in Cotton and Anthes (1989) and Straka (2009). A comparison of various microphysics schemes and a recent development can be found in Khain et al. (2015) and Tsai and Chen (2020), respectively. The ventilation effect, the focus of our study in this paper, is also parameterized. Due to the complexity of hydrometeors, the ventilation parameterizations are often formulated based on a few experimental and/or observational data under limited atmospheric conditions, or computational results of idealized hydrometeors that cover a small subset of real situations in clouds. The incompleteness of data source will certainly introduce uncertainties in the final simulation results of cloud models. In addition, as we have indicated above, parameterization represents simplification, and simplification inevitably introduces errors which may be small or large. These errors will also eventually pass on to the simulation results of cloud models which use these parameterizations adding to further uncertainties. It is therefore important to understand the sources of these possible uncertainties by studying the impact of the parameterizations used.

In order to assess how large, the terminal errors can be and therefore how reliable the simulation results are due to the parameterization, one useful way is to perform sensitivity studies. One way of doing the sensitivity study is forming a new parameterization via changing the magnitude of the factor in concern, in this case the ventilation. Then run the model with the new parameterization and compare the results with that performed with the original parametrization to see how sensitive the model results are to different parameterizations. This is what we will do and we will focus on the impact on the simulated storm's life span in this study. In the following sections, we will first review the ventilation parameterization and then perform the sensitivity study as outlined above. Then we will make some analyses on the possibly reasons about the sensitivity. Conclusions will be presented at the end.

2. THE VENTILATION COEFFICIENT

Mathematically, the ventilation coefficient is defined as the ratio of the mass growth rate $(\partial m / \partial t)$ of a moving hydrometeor to that of a stationary hydrometeor $(\partial m / \partial t)_0$:

$$\overline{f}_v = \left(\frac{\partial m}{\partial t}\right) \Big/ \left(\frac{\partial m}{\partial t}\right)_0 \tag{1}$$

where m is the mass of the hydrometeor and $\overline{f}_v$ the mean ventilation coefficient (Wang 2013). The latter is called mean because it is the average of the local ventilation coefficients over the surface of the hydrometeor and the local ventilation coefficients can be different at different surface points. The term "ventilation coefficient" hereafter will represent the "mean ventilation coefficient".

The precise determination of $\overline{f}_v$ requires either precise experimental measurements in a controlled laboratory such as those performed in a vertical wind tunnel (e.g., Beard and Pruppacher 1971) or detailed calculations utilizing computational fluid dynamical methods (e.g., Ji and Wang 1999; Cheng et al. 2014, 2015; Nettesheim and Wang 2018; Wang and Chueh 2020). In order to be implemented into cloud models, the ventilation coefficients, either measured or calculated by CFD models, are expressed in algebraic form as a function of either the hydrometeor size or Reynolds number or some other quantities characterizing the motion and size of the hydrometeor.

Often a dimensionless number X as defined below is used as the dependent variable in the parameterization (Wang 2013, 2021):

$$X = N_{Sc}^{1/3} N_{Re}^{1/2} \tag{2}$$

where N_{Sc} and N_{Re} are the Schmidt number and Reynolds number as defined below:

$$N_{Sc} = v / D_v \tag{3}$$

$$N_{Re} = d u_\infty / v \tag{4}$$

Here v is the kinematic viscosity of air, D_v the diffusivity of water vapor in air, d the dimension of the hydrometeor, and u_∞ the terminal fall speed of the hydrometeor. The ventilation parameterization is usually of the following polynomial form (see Pruppacher and Klett 1997; Wang 2013, 2020 for throughout reviews):

$$\overline{f_v} = c_0 + c_1 X + c_2 X^2 + ... \tag{5}$$

where c_0, c_1, and c_2 are coefficients.

Usually one or two terms on the right-hand side are adequate. Sets of commonly referenced values of coefficients were given by Beard and Pruppacher (1971) and Pruppacher and Rasmussen (1979) for raindrops, and Hall and Pruppacher (1976) for ice crystals. The coefficients are summarized in Table 1. More recently, Cheng et al. (2014) utilized computational fluid dynamics to solve the unsteady Navier-Stokes equation around the large spherical hailstones of various sizes at certain atmospheric condition. Wang and Chueh (2020) adopted the similar approach to conduct ventilation experiments on lobed hailstones of many shapes. These recent numerical experiments have explored a new territory where the Reynolds numbers are pushed far beyond the early studies were able to reach. The parameterizations of the spherical hails and one represented lobed hails are also included in Table 1.

The modulation of the ventilation effect on mass growth rate caused by diffusion/deposition of water vapor on a spherical hydrometeor of diameter, d, is given by (Rutledge and Hobbs 1984)

$$\frac{\partial m(d)}{\partial t} = \frac{2\pi d(S-1)}{A' + B'} \overline{f_v} \tag{6}$$

where S is the saturation ratio over the specified hydrometeor, and A' and B' are thermodynamics parameters (Pruppacher and Klett 1997). The particle size distribution is commonly assumed to follow the gamma function $N(D) = N_0 D^\mu e^{-\lambda D}$, where N_0, μ, and λ are the intercept, slope, and shape parameters, respectively. The terminal fall speed, which is also size dependent, is parameterized in the form of

$u_\infty = ad^b$. Like N_0, μ, and λ, a and b are species specified parameters. A general form of depositional/diffusion growth is given by integrating the mass growth rate over the size distribution function:

$$\left(\frac{\partial q}{\partial t}\right)_{dep} = \frac{2\pi d(S-1)}{A' + B'}\left[c_0 \frac{\Gamma(\mu+2)}{\lambda^{\mu+2}} + c_1\alpha \frac{\Gamma\left(\mu+\frac{b}{2}+\frac{5}{2}\right)}{\lambda^{\frac{b}{2}+\frac{5}{2}}} + c_2\alpha^2 \frac{\Gamma(\mu+b+3)}{\lambda^{b+3}} + ...\right] \tag{7}$$

where

$$\alpha = N_{Sc}^{1/3}\left(\frac{a}{v}\right)^{1/2} \tag{8}$$

Many parameterizations of mass growth rate share this form (Rutledge and Hobbs 1984; Reisner et al. 1998; Morrison et al. 2009).

In the present study, we focus on the sensitivity of the ventilation coefficients of large hydrometeors, namely, raindrops, snow aggregates, and hail, as smaller hydrometeors such as cloud drops and cloud ice have much smaller ventilation effect and would likely contribute little to the sensitivity. We believe the sensitivity of ventilation effect on cloud model simulations has not been performed before and this study should contribute to useful insight on this matter.

3. WISCDYMM-II MODEL DESCRIPTION AND EXPERIMENTAL SETTINGS

The cloud model we used throughout this study for testing the ventilation sensitivity is one developed in P. K. Wang's research group at the University of Wisconsin-Madison, the Wisconsin Dynamical Microphysical Model double moment version (WISCDYMM-II). WISCDYMM-II adopts fully compressible non-hydrostatic moisture equations (Klemp et al. 2007), in contrast to its predecessor WISCDYMM (Straka 1989; Johnson et al. 1993, 1994; Lin and Wang 1997; Wang 2003), which is quasi-compressible. Furthermore,

Table 1. The ventilation coefficients for raindrops, ideal ice crystals, spherical and lobed hailstones. See the context for the references.

hydrometeor	c_0	c_1	c_2	c_3
Raindrops	0.78	0.308		
Ice crystals	0.86	0.28		
Spherical hails	-11.7501	0.3865	0.00063	
Lobed hails (6uv-long)	9.533	-0.2463	0.00547	-4.589×10^{-6}

the model uses a double moment scheme as given in Morrison et al. (2005, 2009) (hereafter called the Morrison scheme) to predict both the mixing ratio and the number concentration instead of the single moment scheme used in the previous version. The prognostic variables in Morrison scheme include vapor, cloud water, cloud ice, rain, snow, and hail/graupel. In this study, hail is chosen over graupel as the dense precipitating ice, and the number concentration of cloud water is prognosticated. On the other hand, the model also adopts the 1.5 order turbulence closure to account for the sub-grid eddy mixing as the previous version. WISCDYMM-II has been used successfully in a study of the storm top internal gravity wave breaking (Wang et al. 2015).

The initial conditions we adopt for this study is the sounding recorded right before the mid-latitude supercell storm took place on 2 August 1981 in southeastern Montana (see Fig. 1) by the cooperative convective precipitation experiment (CCOPE) observational network as detailed by Knight (1982). The sounding shows a high value of convective available potential energy (CAPE) close to 3313 J kg^{-1}, which is an indication of strong instability in the atmosphere. In addition, a low lifted index of -9.4°C also favors development of severe thunderstorm with lifting mechanism. The strong vertical wind shears near the ground level (as shown in the wind barbs) indicate that a rightward-moving storm is likely to occur. This supercell has been widely studied since then (Wade 1982; Miller et al. 1988; Johnson et al. 1993,

1994; Wang et al. 2008; Fernández-González et al. 2016). This supercell had been simulated by Johnson et al. (1993, 1994) who had performed detailed analyses of the simulation results using the older version WISCDYMM. We follow the methodology of these previous studies and initiate the storm through perturbing the temperature field confined by a warm ellipsoidal bubble near the surface level. The instability of the warm bubble would evolve into a supercell.

Among the five hydrometeors, rain, snow, and hail are the categories involved in the process of ventilation which includes condensation/evaporation and deposition/sublimation. The ventilation effect for small hydrometeors (< 50 μm) is usually considered not significant and can be neglected in most cases (Pruppacher and Klett 1997). Therefore, the ventilation effect for cloud water and cloud ice are not considered in the present study.

Morrison et al. (2009) treated snow and graupel/hail as the ideal ice crystals and adopted the same ventilation coefficients given by Hall and Pruppacher (1976). However, according to the parameterization given by Cheng et al. (2014), for spherical hailstones of diameters in the range of 3.5 to 10 cm, the ventilation effect can be as 1.5 to 2 times larger than the classic parameterization projected. The deviations from the ideal ice crystal for lobed hails are even larger (Wang and Chueh 2020). Different habits of snow crystals could also cause the ventilation parameterizations to depart from the ideal one (Ji and Wang 1999; Nettesheim
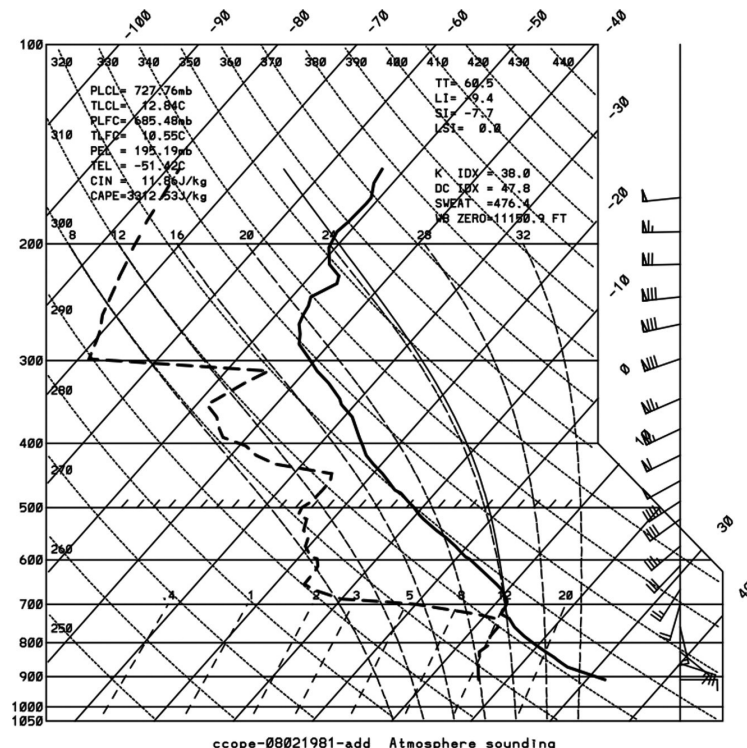
Fig. 1. Skew T – log P diagram at 1746 MDT on 2 August 1981 in Knowlton, Montana. The solid and dashed curves indicate the temperature and the dew point, respectively. The thin solid line represents an equivalent potential temperature of 352 K.

and Wang 2018). As for the raindrops, like ice crystals, the parameterization is based on the assumption that their shapes are spherical. However, observations (Wang 2021) shown that during falling the shape could be distorted and hence affects the ventilation effect.

Our objective is not to seek sophisticated representations of ventilation parameterizations and their contributions to the accuracy of numerical weather predictions. Instead, we test how altering the ventilation coefficients would affect the evolution and structure of the storm. The former will be our goal in the near feature.

We systematically adjust the ventilation coefficients through multiplying a common factor, Z, which we call the amplification factor of the ventilation effect, for all the three hydrometeors. Thus, the adjusted ventilation coefficient is of the form $Z\bar{f}_v$. We have systematically changed the values of Z between 0.5 and 2, however, we will report the simulation results of $Z = 0.5$, 1, and 2 as they are representative enough for us to understand the sensitivity of both reducing and enhancing the ventilation coefficient in a cloud model. $Z = 1$ represents the control case where the ventilation scheme is exactly the same as in Morrison et al. (2009) to which the results of reduced ($Z = 0.5$) and enhanced ($Z = 2$) cases will be compared.

The computational domain of the simulations is 160 × 160 × 25 km³ and the grid resolution is 500 m horizontal and 200 m vertical, from surface to top throughout. The temporal resolution is set at 2 sec. We ran the simulation for 5 hours all the cases. We adopt a storm-following methodology where we shift the domain every time step to align an anchor point (40 km west to the center of the frame) to the mass center of convective cell(s) so as to keep the simulated storm in the center of the computational domain.

4. RESULTS AND ANALYSIS

Figure 2 shows the top-view snapshots of the temporal evolution of the three simulated storms for $Z = 0.5$ (left), $Z = 1$ (center), and $Z = 2$ (right). The storms are visualized by the iso-surfaces of hydrometeor mixing ratio of 0.1 g kg⁻¹. Different color represents different hydrometeors: grey for total hydrometeor mixing ratio (thus representing approximately the visible cloud outer boundary), yellow for rain, purple for snow and blue for hail. Note that these are 3-dimensional plots viewed from above but not horizontal cross sections at a specified altitude. These isosurfaces are shown every 30 min from $t = 30$ min to 300 min. As mentioned before, the storms appear to be stationary because of the storm-following reference frame we used. In reality, they all move northeast with direction and speed following approximately the mid-level winds.

At $t = 30$ min, all three storms look quite similar – the anvil starts to stretch to the downwind (right-hand) side and the overshooting top emerges. The similarity of all three

indicates that the sensitivity on ventilation is not obvious mainly because the quantities of large hydrometeors (rain, snow, and graupel/hail) are not substantial enough to cause noticeable ventilation impact. At $t = 60$ min, however, the ventilation effect starts to become apparent. We see that, while the reduced case storm continues to evolve larger but still remains as a single cell, the $Z = 1$ and $Z = 2$ cases exhibit "storm-splitting" behavior manifested by a smaller storm cell developed to the north (upper) side of the original storm. The splitting is the more obvious in the $Z = 2$ case. This is a clear sign that the ventilation effect is operating in influencing the storm development as will be explained later.

After $t = 90$ min, the three storm cases evolve quite differently. It appears that the $Z = 0.5$ case peaks at $t \sim 90$ min and then starts to dissipate. Its cold cloud top disappears totally after $t = 120$ min and continues to dissipate thereafter and vanish eventually. The control case lasts somewhat longer but the eventual dissipation is obvious after $t = 180$ min.

In contrast, the enhanced case ($Z = 2$) continues to evolve. It splits into two storms at $t \sim 80$ min (not shown) and the splitting is very obvious at $t = 90$ min (Fig. 2): the one to the north continues to grow larger while the one to the south initially becomes smaller but later re-develop to become slightly larger at $t = 240$ min. At the same time, the north one starts to develop into multiple cell structure akin to splitting and expands toward the south. Both cells continue to enlarge and eventually merge to form a multicellular system that prevails the entire domain.

The above observations show at least two points: (1) the enhanced ventilation case leads to a longer-lived storm than the other two cases; and (2) this enhanced case exhibits obvious storm splitting feature whereas the reduced and control cases show non- or short-lived splitting. To understand these points further, we plot the time evolution of the cloud total volume and total mass of condensates (sum of the mass of all hydrometeors) as shown in Fig. 3.

Figure 3a shows that the evolutions of total condensate mass are nearly identical for all three cases in the first 30 min. This is not surprising as the first 30 min is usually the spin up time of the model and the simulated cloud just reach steady state and the total masses of the condensates are not large enough to affect he cloud dynamics. There are slight differences among the 3 cases in $t = 30$ - 80 min with the reduced case having the largest mass followed by the control and enhanced cases in that order. After 80 min, the reduced and control cases begin to dwindle and the reduced case dissipates first followed by the control case whereas the enhanced case continues to develop larger.

Figure 3b shows the evolutions of total cloud volumes for all three cases. The features are nearly identical to that shown in Fig. 3a although the differences in magnitude at $t = 30$ - 80 min can be more clearly seen. The similarity of the three cases in Fig. 3 in the first 80 min indicates that the ventilation effect would not affect the storm size at least
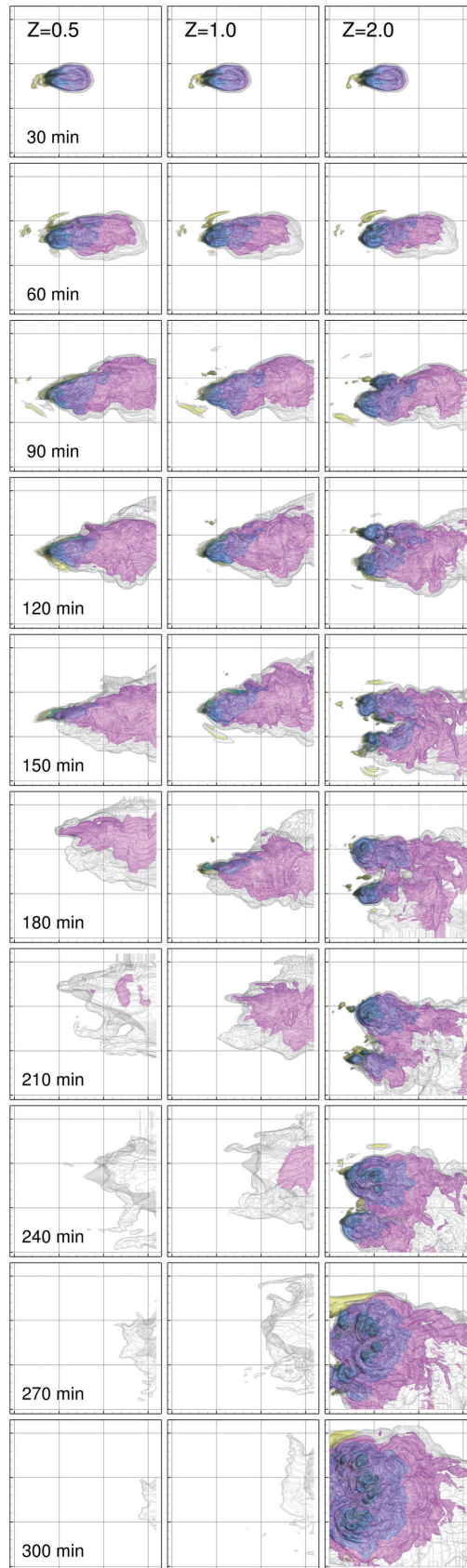
Fig. 2. The top-view snapshots of the temporal evolution of the three storms. The time sequences are arranged from the top row to the bottom with 60 min separations, whereas the ventilation adjustments are Z = 0.5, 1, and 1.5 from the left column to the right. The spatial dimensions are 160 km in both X- and Y-directions, with grid spacing of 20 km. The iso-surfaces of grey, yellow, purple and blue enclose the total hydrometeors, rain, snow, and hail, respectively.
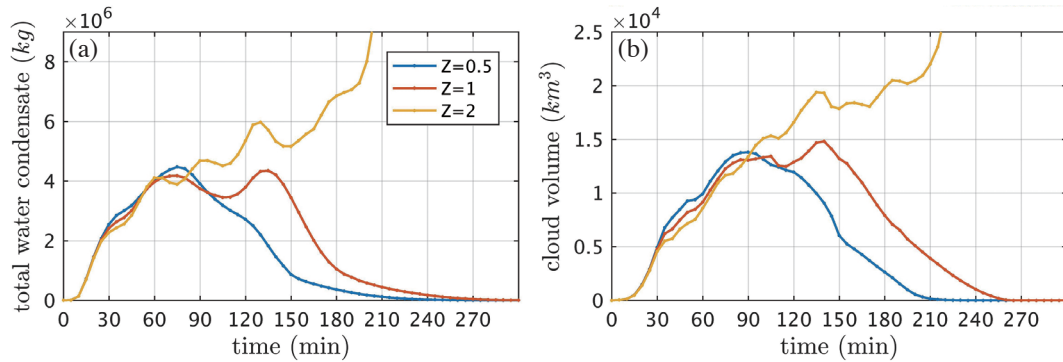
Fig. 3. The temporal evolution of (a) the total mass of the hydrometeors averaged over the entire simulation domain, and (b) the volume occupied by the cloud body. The blue, red, and yellow curves represent the cases of Z = 0.5, 1, and 1.5, respectively.

initially. The enhanced case becomes larger only later as the storm splits.

In order to investigate further, we plot the time evolution of the domain-averaged density of each hydrometeor category as shown in Fig. 4. Remember that only rain, snow and hail are the ventilation-affected categories. The other categories (vapor, cloud water, and cloud ice) are not affected directly by ventilation, so the impact on them is only indirect, namely, as a result of the total water conservation.

Here we see that in the first 30 min all moisture categories of the three cases behave very much the same, just like that in Fig. 3 and the reason is mostly the same. In $t \sim 30 - 80$ min, the reduced case generally has the highest density of both rain and snow, followed by the control and enhanced case, although the enhanced case fluctuates somewhat in the latter half of this period. The hail density evolution, on the other hand, shows some fluctuations: in 30 - 45 min, the abundance order is: reduced > control > enhanced whereas in 50 - 70 min, the order is reversed: it becomes: enhanced > control > reduced. This appears to show that, the higher ventilation, the greater the fluctuation and this leads to the greatest fluctuation for the enhanced case. Since the ventilation effect impacts both the positive and negative growth of hydrometeors, large ventilation coefficient may result in large evaporation, sublimation, and melting (and hence the reduction of density) that overcompensates the ventilated growth during the heavy precipitation stage of the storm leading to the reduction of density, and vice versa. This is likely why the yellow curve (enhanced case) fluctuates most in all moisture categories.

The evolution curves of rain and cloud water are associated closely with hail evolution, as hail is mainly produced by the accretion of supercooled cloud water whereas rain can be produced when hail melts. Likewise, cloud water and rain can also be produced when snow melts. The relation appears to be most obvious in the enhanced case (yellow curves).

The evolution of snow appears to be strongly linked

to that of the cloud ice, although the latter is a not affected by ventilation. It is true that altering the ventilation effect will change the latent heat released by ventilation categories which, in turn, alters the temperature and affects the formation rate of cloud ice, and this makes the interpretation of the link somewhat complicated. However, our results show that the evolution of cloud ice, among the non-ventilation categories, nearly parallels that of snow. We conclude that the aggregation of cloud ice to form snow is probably the most active snow formation processes.

The cloud water evolution curve is associated with many processes, including autoconversion, evaporation, riming and melting of snow and hail. In Morrison scheme, melting of hail/graupel either forms rain, or evaporates in subsaturation. It is not a direct source of forming cloud water. The varying of cloud water in response to the change of ventilation effect could come from the indirect paths associating with the precipitation particles. For example, in the period between the 30 and 70 min, the amounts of the rain and snow are smaller in cases of larger ventilation effect. It results in less accretion/collection of cloud water by rain and snow, and greater amount of cloud water could survive. However, cloud water appears to be most closely related to the hail category which is most obvious in the enhanced case. The cloud water evolution curve of the enhanced case appears most similar to that of the hail evolution but with a ~10 min lead time, suggesting that the cloud water is consumed by riming to form hail.

Figure 4 shows that, aside from the higher fluctuations in the curves of enhanced case, there appears to be no obvious sensitivity of the hydrometeor evolution to ventilation effect. And these curves do not explain why the reduced case should dissipate first.

Next, we examine the vertical distribution of the hydrometeors. Figure 5 shows the x-z view of the 3-dimensional structures of storms (viewed from the south). It includes iso-surfaces of 0.1 g kg^{-1} mixing ratio of rain (yellow), hail (blue), and snow (purple) in the cloud for all three cases.

In this view, the time evolution of the vertical distributions of each hydrometeor category becomes clearer. The first 30 min all three cases look similar. But at $t = 60$ min, the rain and hail isosurfaces in the reduced case (left column) have already developed very wide distributions in the low level and reached the surface. Such heavy rainfall and hailfall would be accompanied by strong downdraft that tends to cut off the flow of unstable moist air near the surface to enter the storm center. Without the replenishment of unstable moist air, the storm quickly weakens and dissipates. In contrast, the same isosurfaces of the control case reached at a similar stage only at $t \sim 90$ min, and hence dissipates later than the reduced case by about 30 min.

The enhanced case has never reached such a stage especially from the hail point of view. The 0.1 g kg^{-1} hail isosurface almost never reaches the surface. Whereas the 0.1 g kg^{-1} rain isosurface does reach surface, the total rainfall is much smaller than both the reduced and control cases. This implies that its downdraft strength is also smaller than the former two and thus would not cut off the continuous supply of unstable surface air, hence the longer life span of the storm.

Figure 6 shows the x-z view of the enhanced case where the south and north branches are separated by an east-west cross section that cuts through the weakest link between them. More detail of the split north cell is further

revealed in Fig. 6. The top right panel indicates the rainfall (yellow color) in the north cell is just about started since it has not spread out the base of the cell. The core of the cell containing rain and hail is in irregular shape comparing with the core of mother cell in its early developing stage (see the top right panel in Fig. 2). The anvil, however, is extended form the mother cells due to the way we separate the north cell from the south. At 120 min, the north part of the storm evolved a wider base containing rain and hail than the south part although the cloud top is still about 2 km lower. At the same time, the size of the south cell starts to shrink. Its cold cloud top collapses shortly from 150 min but re-emerge at 180 min. The north cell continues to develop both vertically and horizontally. Its core pushes higher and higher with a cloud top reaches 16 km at 150 min and hail beyond 15 km at 210 min. The volume containing rain and hail become wider in horizontal as well. In general, hail reaches lower levels in north than in the south indicating that hails might grow larger in the south than the north to survive in conditions of melting and sublimation.

Figures 5 and 6 also show interesting aspect of overshooting of the cloud tops. Although the snapshots of every 30 min might not capture fine detail of the developments of the overshooting, the trend against adjusting the ventilation effect is clearly revealed. In the early stage of developing
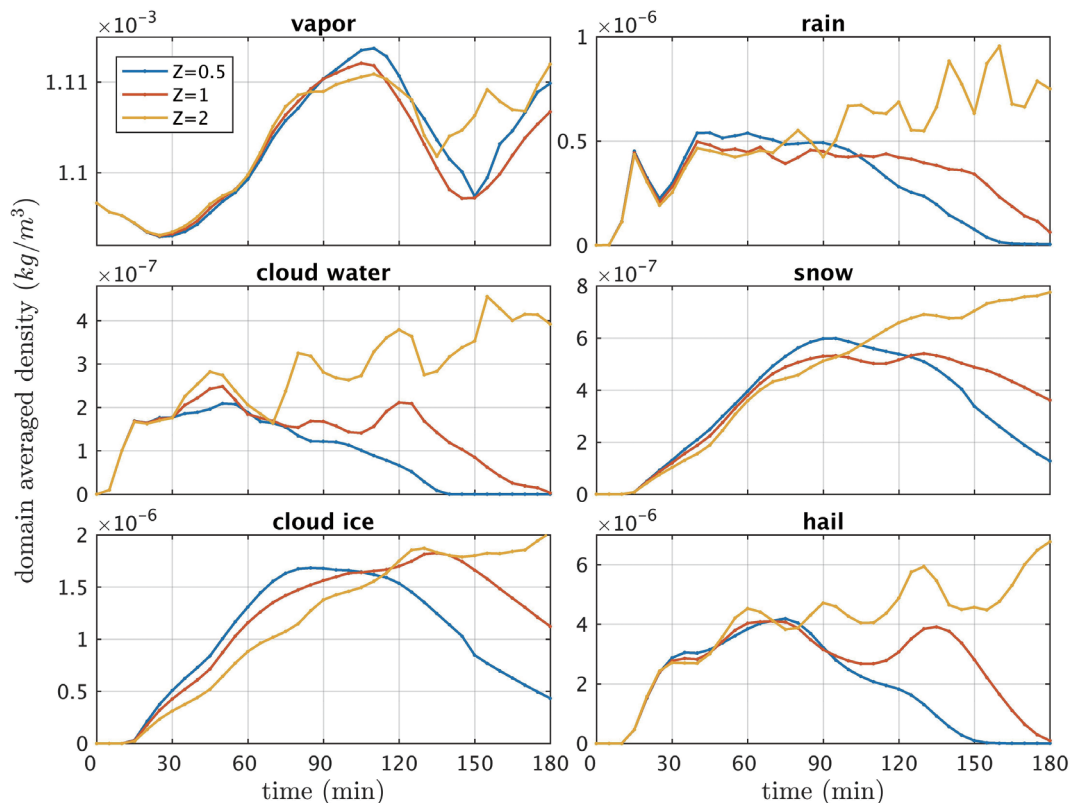
Fig. 4. The temporal evolutions of the averaged densities in the simulation domain. The six species, namely vapor, cloud water, cloud ice, rain, snow, and hail are shown in different panels for all the three cases in the color codes the same as Fig. 3.
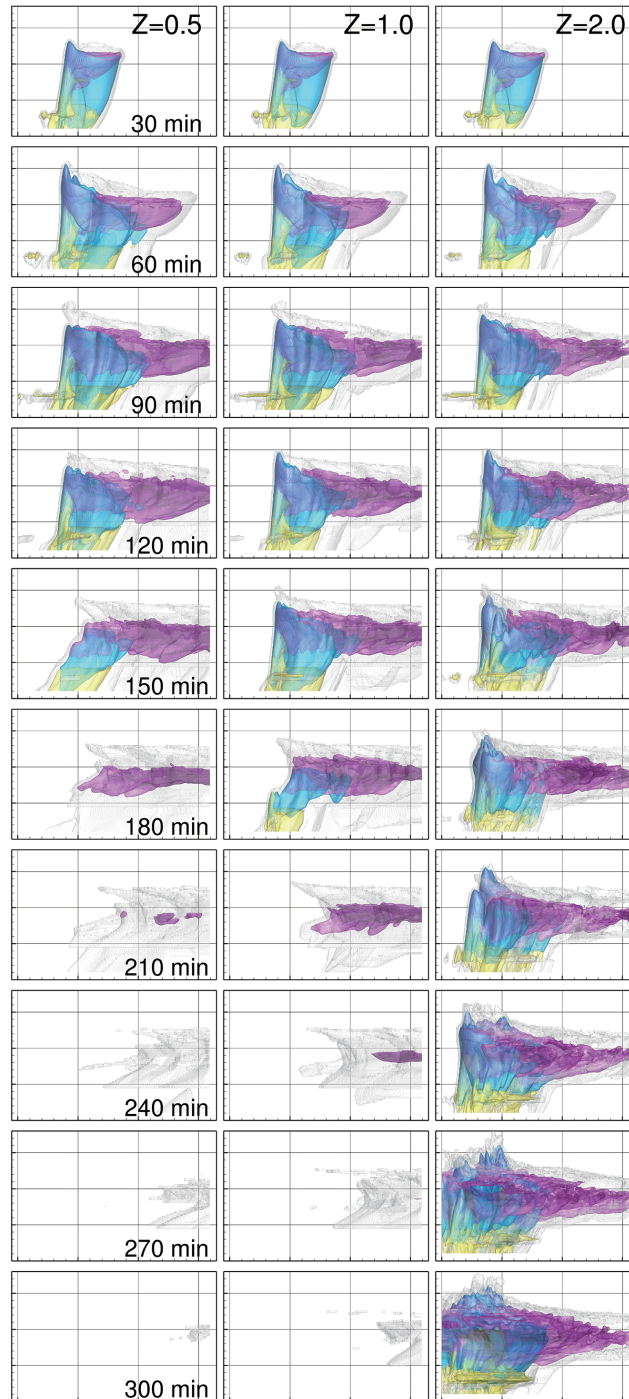
Fig. 5. The side-view snapshots of the temporal evolution of the three storms. In order to reveal the structure, the vertical scale is enlarge such that the vertical grid spacing is 5 km (vs. 20 km in the horizontal). The other details are the same as Fig. 2.
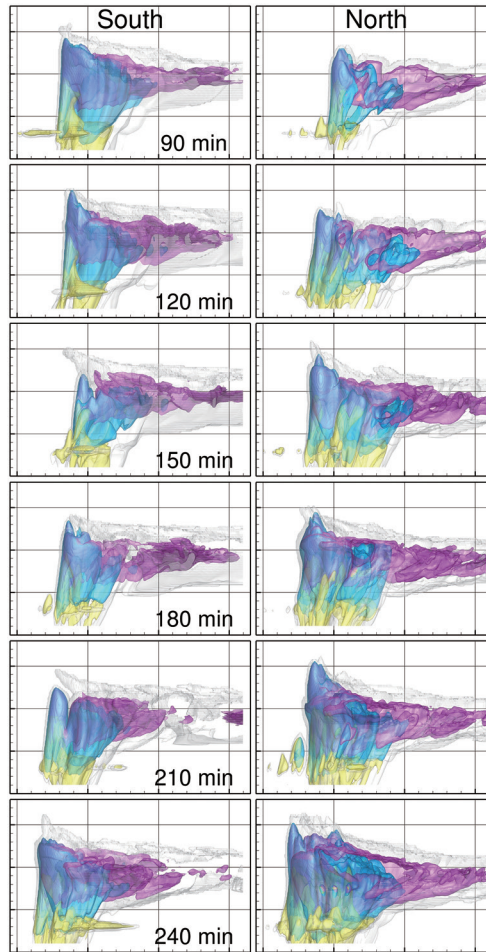
Fig. 6. The side-view snapshots of the south (left column) and north (right column) cells in the enhanced case. The south and north branches are separated by an east-west vertical cross section located at 67.5, 90, 60, 70, 60, and 50 km from the south boundary of the domain for 90, 120, 150, 180, 210, and 240 min, respectively. The other details are the same as Fig. 2.

the overshooting tops, hail, snow and cloud ice keep raising upward, with cloud ice floating above the others, to from a dome. The panels of 60 min represent typical profiles of this phase, where the tops of the three cases reach about the same altitude (near 16 km). What follows is that hail and snow fall, but cloud ice spouts from the dome to form plume. The snapshots of 90 min show typical profiles of this phase where hail and snow drop to lower altitudes (12 - 14 km). Around this stage, the development of overshooting completes a cycle. The further development strongly dependents on the ventilation effect. In the case of reduced ventilation, the plume collapses as shown in the 120 min panel in Fig. 5 followed by disruptions of hail and snow at 150 min. In control run, another cycle occurs with two distinct phases shown in panels of 120 and 150 min, followed by the collapse of the overshooting dome (180 min). In the enhanced case, the overshooting re-emerges in the south branch during the period between 120 and 150 min. At the same time, the north branch matures and forms overshooting dome since 120 min. As shown in Fig. 6 that the

developing the overshooting persists to 210 min. From 240 min afterward, multiple cells form and overshooting tops at different phases occur simultaneously.

Figure 7 shows the vertical distributions of mixing ratio for rain (upper row), snow (middle row), and hail (lower row) of the three cases at 6 different time steps" 30, 60, 90, 120, 150, and 180 min. We immediately see that in $t = 60$ - 120 min at the surface level the rain is the largest for the reduced case (Fig. 7a) followed by the control (Fig. 7b) and the enhanced case (Fig. 7c). The heavy rain in the low level of the reduced case cuts off the inflow of moist unstable air into the main updraft core that is necessary for the storm to continue to develop. Without such inflow, the storm dissipates rapidly. We believe this is the main reason why the reduced case is the most short-lived.

The reason why the reduced case has the largest rainfall must be due to the reduced evaporation rate so that large number of raindrops survives to the surface when they fall. In contrast, the small rainfall amount near the surface for the enhanced case is clearly due to the excessive
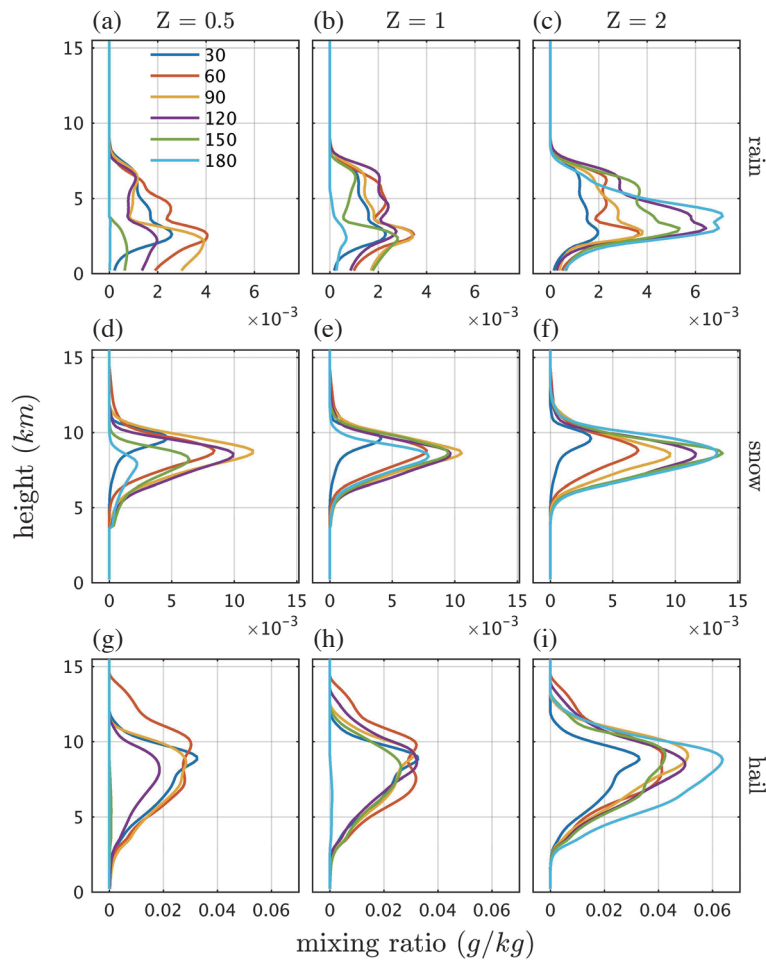
Fig. 7. The vertical profiles of mixing ratio for rain (upper row), snow (middle row), and hail (lower row); and for cases Z = 0.5 (left column), 1 (middle column), and 2 (right column). In each panels, the time steps at 30, 60, 90, 120, 150, and 180 min are drawn with color codes show in panel (a).

ventilation causing enhanced evaporation that dissipates much rainwater during rainfall. As Fig. 7c shows, most of the rain water remains at higher level at 3 - 5 km height for the enhanced case.

Figure 8 shows the domain averaged precipitation rate of rain and hail at the surface for the three cases. Note that the vertical scale of the rainfall rate is ten times that of the hailfall rate. Again, the reduced case has the largest rainfall and hailfall rates followed by the control case. The enhanced case has the smallest rainfall and hailfall rates. These features corroborate with the vertical distributions as shown in Fig. 7 that the large rainfall of the reduced ventilation case cuts off the supply of unstable moist air causing the storm to dissipates quickly. In contrast, the higher ventilation effect of the control and enhanced cases reduces the rainfall rate and prolongs the storm life span.

Figure 9 shows the maximum downdraft velocity on the lowest level of the three simulated storms as a function of time. It is seen that the maximum downdraft at $t =$

35 min is the largest for the reduced case and the smallest for the enhanced case that corroborates our observations in Figs. 7 and 8.

The storm splitting behavior of the enhanced case shown in Fig. 2 (right-hand column) deserves some discussion. Many severe storms in US Great Plains exhibit storm splitting behavior. The most typical is that a mature storm is split into a northern cell and southern cell as the storm moves eastward, and eventually the northern one weakens and dissipates while the southern one (the right moving one) may continue to grow and even split again (Doswell and Brooks 2002). In view of the high concentration of raindrops in the midlevel for the enhanced case as seen in Fig. 7, one may suspect that the splitting is due to the large precipitation loading in the midlevel. However, according to the study by Rotunno and Klemp (1982), it is the shear-induced pressure gradient that is the main factor promoting the splitting. We will conduct a follow-up study to investigate this point for all three cases in the near future.
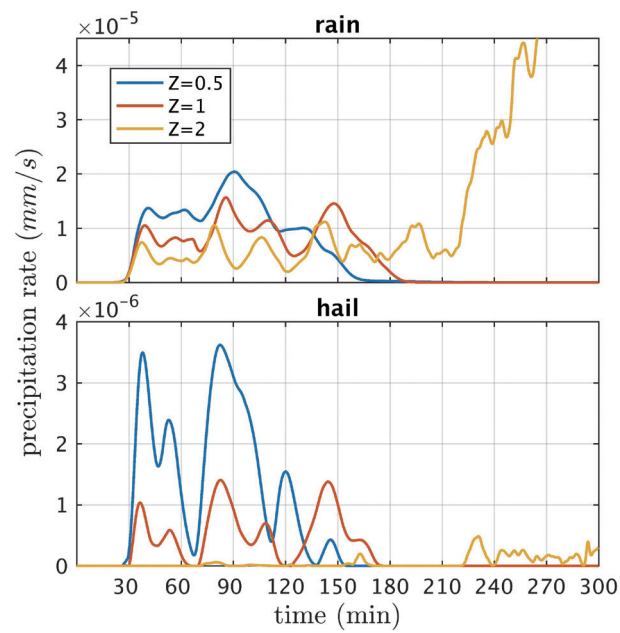
Fig. 8. Average precipitation rate of rain and hail measured in the area covered by the entire simulation domain. The color codes indicated the three cases are the same as Fig. 3.
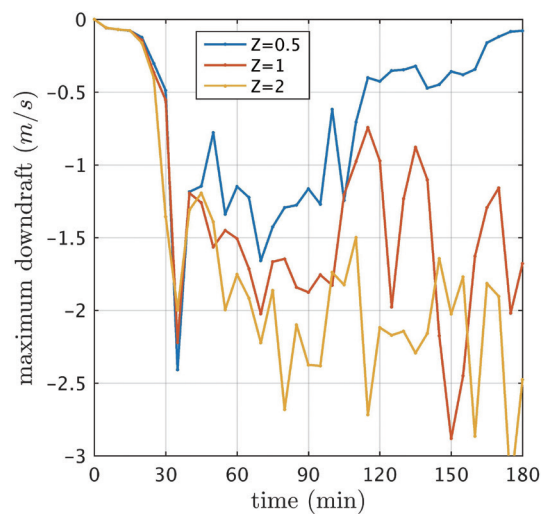
Fig. 9. The temporal evolutions of the maximum downdraft on the lowest level of the simulation domain. The color codes are the same as Fig. 3.

5. CONCLUSIONS

We performed a sensitivity study utilizing cloud model simulations to investigate how different ventilation parameterizations may impact the life span of the simulated storms. We used the widely adopted ventilation parameterizations as the control case and investigated the sensitivity of reduced ventilation, normal and enhanced ventilation effect by multiplying a constant factor Z so as to represent the half, normal, and double ventilation. The simulated storms with different ventilation coefficients exhibit distinctly different behaviors and most obviously in the storm life span. Our results show that with reduced ventilation, the raindrop concentration becomes very large near the surface producing strong downdraft that cuts off the low-level inflow of unstable moist air into the storm and the storm therefore dissipates the fastest. In contrast, with enhanced ventilation, the raindrops falling through subsaturated air evaporated quickly before they reach lower level and thus are unable to cut off the incoming surface air and the storm continues to grow larger. This study thus demonstrates that the storm simulation results are sensitive to the parameterization of ventilation.

We have also outlined the relations between the evolutionary histories of different hydrometeor categories under various ventilation scenarios based on qualitative examination of the simulation results. To substantiate these interpretations, we need to perform studies on the thermodynamics of each microphysical process involved. We plan to perform such studies in the near future.

As indicated previously, our knowledge of the ventilation coefficients of falling hydrometeors are inadequate especially that of large ice hydrometeors. The theoretical ventilation coefficients of smooth and lobed hailstones are only recently become available (Cheng et al. 2014; Wang and Chueh 2020) and they have not been properly parameterized for application in cloud models. The ventilation coefficients for graupel and snowflakes are not yet available at this moment. The future generation of cloud models will need to implement these accurate ventilation parameterizations to obtain reliable simulation results.

REFERENCES

Beard, K.V. and H. R. Pruppacher, 1971: A Wind Tunnel Investigation of the Rate of Evaporation of Small Water Drops Falling at Terminal Velocity in Air. *J. Atmos. Sci.*, **28**, 1455-1464, doi: 10.1175/1520-0469(1971)028<1455:AWTIOT>2.0.CO;2. [Link]

Cheng, K.-Y., P. K. Wang, and C.-K. Wang, 2014: A Numerical Study on the Ventilation Coefficients of Falling Hailstones. *J. Atmos. Sci.*, **71**, 2625-2634, doi: 10.1175/JAS-D-13-0229.1. [Link]

Cheng, K.-Y., P. K. Wang, and T. Hashino, 2015: A numerical study on the attitudes and aerodynamics of freely falling hexagonal ice plates. *J. Atmos. Sci.*, **72**, 3685-3698, doi: 10.1175/JAS-D-15-0059.1. [Link]

Cotton, W. and R. Anthes, 1989: Storm and Cloud Dynamics, 1st Edition, Academic Press, San Diego, 883 pp.

Doswell, C. A. and H. E. Brooks, 2002: Lessons Learned from the Damage Produced by the Tornadoes of 3 May 1999. *Weather Forecast.*, **17**, 611-618, doi: 10.1175/1520-0434(2002)017<0611:LLFTDP>2.0.CO;2. [Link]

Fernández-González, S., P. K. Wang, E. Gascón, F. Valero, and J. L. Sánchez, 2016: Latent cooling and microphysics effects in deep convection. *Atmos. Res.*, **180**, 189-199, doi: 10.1016/j.atmosres.2016.05.022. [Link]

Fujita, T. T., 1978: Manual of downburst identification for Project NIMROD. SMRP Research Paper No. 156, University of Chicago, 104 pp.

Hall, W. D. and H. R. Pruppacher, 1976: The Survival of Ice Particles Falling from Cirrus Clouds in Subsaturated Air. *J. Atmos. Sci.*, **33**, 1995-2006, doi: 10.1175/1520-0469(1976)033<1995:TSOIPF>2.0.CO;2. [Link]

Ji, W. and P. K. Wang, 1999: Ventilation Coefficients for Falling Ice Crystals in the Atmosphere at Low-Intermediate Reynolds Numbers. *J. Atmos. Sci.*, **56**, 829-836, doi: 10.1175/1520-0469(1999)056<0829:VCFFIC>2.0.CO;2. [Link]

Johnson, D. E., P. K. Wang, and J. M. Straka, 1993: Numerical simulations of the 2 August 1981 CCOPE supercell storm with and without ice microphysics. *J. Appl. Meteorol. Climatol.*, **32**, 745-759, doi: 10.1175/1520-0450(1993)032<0745:NSOTAC>2.0.CO;2. [Link]

Johnson, D. E., P. K. Wang, and J. M. Straka, 1994: A study of microphysical processes in the 2 August 1981 CCOPE supercell storm. *Atmos. Res.*, **33**, 93-123, doi: 10.1016/0169-8095(94)90015-9. [Link]

Khain, A. P., K. D. Beheng, A. Heymsfield, A. Korolev, S. O. Krichak, Z. Levin, M. Pinsky, V. Phillips, T. Prabhakaran, A. Teller, S. C. van den Heever, and J.-I. Yano, 2015: Representation of microphysical processes in cloud-resolving models: Spectral (bin) microphysics versus bulk parameterization. *Rev. Geophys.*, **53**, 247-322, doi: 10.1002/2014RG000468. [Link]

Klemp, J. B., W. C. Skamarock, and J. Dudhia, 2007: Conservative split-explicit time integration methods for the compressible nonhydrostatic equations. *Mon. Weather Rev.*, **135**, 2897-2913, doi: 10.1175/MWR3440.1. [Link]

Knight, C. A., 1982: The Cooperative Convective Precipitation Experiment (CCOPE), 18 May-7 August 1981. *Bull. Amer. Meteorol. Soc.*, **63**, 386-398, doi: 10.1175/1520-0477(1982)063<0386:TCCPEM>2.0.CO;2. [Link]

Lin, H.-M. and P. K. Wang, 1997: A Numerical Study of Microphysical Processes in the 21 June 1991 Northern Taiwan Mesoscale Precipitation System. *Terr. Atmos. Ocean. Sci.*, **8**, 385-404, doi: 10.3319/TAO.1997.8.4.385(A). [Link]

Miller, L. J., J. D. Tuttle, and C. A. Knight, 1988: Airflow and Hail Growth in a Severe Northern High Plains Supercell. *J. Atmos. Sci.*, **45**, 736-762, doi: 10.1175/1520-0469(1988)045<0736:AAHGIA>2.0.CO;2. [Link]

Morrison, H., J. A. Curry, and V. I. Khvorostyanov, 2005: A new double-moment microphysics parameterization for application in cloud and climate models. Part I: Description. *J. Atmos. Sci.*, **62**, 1665-1677, doi: 10.1175/JAS3446.1. [Link]

Morrison, H., G. Thompson, and V. Tatarskii, 2009: Impact of cloud microphysics on the development of trailing stratiform precipitation in a simulated squall line: Comparison of one- and two-moment schemes. *Mon. Weather Rev.*, **137**, 991-1007, doi: 10.1175/2008MWR2556.1. [Link]

Nettesheim, J. J. and P. K. Wang, 2018: A Numerical Study on the Aerodynamics of Freely Falling Planar Ice Crystals. *J. Atmos. Sci.*, **75**, 2849-2865, doi: 10.1175/JAS-D-18-0041.1. [Link]

Pruppacher, H. R. and J. D. Klett, 1997: Microphysics of Clouds and Precipitation, Kluwer Academic, Dordrecht, 954 pp.

Pruppacher, H. R. and R. Rasmussen, 1979: A wind tunnel investigation of the rate of evaporation of large water drops falling at terminal velocity in air. *J. Atmos. Sci.*, **36**, 1255-1260, doi: 10.1175/1520-0469(1979)036<1255:AWTIOT>2.0.CO;2. [Link]

Reisner, J., R. M. Rasmussen, and R. T. Bruintjes, 1998: Explicit forecasting of supercooled liquid water in winter storms using the MM5 mesoscale model. *Q. J. R. Meteorol. Soc.*, **124**, 1071-1107, doi: 10.1002/qj.49712454804. [Link]

Rotunno, R. and J. B. Klemp, 1982: The Influence of the Shear-Induced Pressure Gradient on Thunderstorm Motion. *Mon. Weather Rev.*, **110**, 136-151, doi: 10.1175/1520-0493(1982)110<0136:TIOTSI>2.0.CO;2. [Link]

Rutledge, S. A. and P. V. Hobbs, 1984: The Mesoscale and Microscale Structure and Organization of Clouds and Precipitation in Midlatitude Cyclones. Xii: A Diagnostic Modeling Study of Precipitation Development in Narrow Cold-Frontal Rainbands. *J. Atmos. Sci.*, **41**, 2949-2972, doi: 10.1175/1520-0469(1984)041<2949:TMAMSA>2.0.CO;2. [Link]

Straka, J. M., 1989: Hail growth in a highly-glaciated central high plains multi-cellular hailstorm. Ph.D. Thesis, The University Of Wisconsin - Madison.

Straka, J. M., 2009: Cloud and Precipitation Microphysics: Principles and Parameterizations, Cambridge University Press, Cambridge, 392 pp, doi: 10.1017/CBO9780511581168. [Link]

Tsai, T.-C. and J.-P. Chen, 2020: Multimoment Ice Bulk Microphysics Scheme with Consideration for Particle Shape and Apparent Density. Part I: Methodology and Idealized Simulation. *J. Atmos. Sci.*, **77**, 1821-1850, doi: 10.1175/JAS-D-19-0125.1. [Link]

Wade, C. G., 1982: A Preliminary Study of an Intense Thunderstorm Which Moved across the CCOPE Research Network in Southeastern Montana. Ninth Conference on Weather Forecasting and Analysis, Am. Meteorol. Soc., Seattle, WA, 388-395.

Wang, P. K., 2003: Moisture plumes above thunderstorm anvils and their contributions to cross-tropopause transport of water vapor in midlatitudes. *J. Geophys. Res.*, **108**, 4194, doi: 10.1029/2002JD002581. [Link]

Wang, P. K., 2013: Physics and Dynamics of Clouds and Precipitation, Cambridge University Press, Cambridge, 467 pp, doi: 10.1017/CBO9780511794285. [Link]

Wang, P. K., 2021: Motions of Ice Hydrometeors in the Atmosphere: Numerical Studies and Implications, Springer Singapore, 176 pp, doi: 10.1007/978-981-33-4431-0. [Link]

Wang, P. K. and C.-C. Chueh, 2020: A numerical study on the ventilation coefficients of falling lobed hailstones. *Atmos. Res.*, **234**, 104737, doi: 10.1016/j.atmosres.2019.104737. [Link]

Wang, P. K., H. Lin, H.-C. Liu, M. Chiruta, and R. E. Schlesinger, 2008: Recent Advances in Research on Micro- to Storm-Scale Ice Microphysical Processes in Clouds. In: Liou, K. N. and M. D. Chou (Eds.), Recent Progress in Atmospheric Sciences: Applications to the Asia-Pacific Region, World Scientific, 419-437, doi: 10.1142/9789812818911_0020. [Link]

Wang, P. K., C.-C. Chueh, and C.-K. Wang, 2015: A numerical study of flow fields of lobed hailstones falling in air. *Atmos. Res.*, **160**, 1-14, doi: 10.1016/j.atmosres.2015.02.013. [Link]